THE JOURNAL OF PHYSICAL CHEMISTRY A

ARTICLE

pubs.acs.org/JPCA

Fewest-Switches Surface Hopping and Decoherence in Multiple Dimensions

Joseph E. Subotnik*

Department of Chemistry, University of Pennsylvania, Philadelphia, Pennsylvania 19104, United States

ABSTRACT: In a recent article (Subotnik, J. E.; Shenvi, N. *J. Chem. Phys.* **2011**, *134*, 24105), we introduced a new approach for incorporating decoherence into the fewest-switches surface-hopping (FSSH) algorithm, titled augmented FSSH (A-FSSH). The A-FSSH algorithm was designed to correct the well-known overcoherence problem in traditional FSSH, and thus allow wave packets on different surfaces to separate naturally subject to different forces. As presented earlier, however, the A-FSSH algorithm was restricted to two electronic states. We now extend the method to more than two electronic states and present several new model problems with multiple electronic and nuclear dimensions. Lastly, starting with the quantum Liouville equation, we rederive and implement the new phase correction suggested by Shenvi (Shenvi, N.; Subotnik, J. E.; Yang, W. *J. Chem. Phys.* **2011**, *135*, 24101) and co-workers for propagating the electronic amplitude along a specified nuclear trajectory and find much improved results in certain cases.

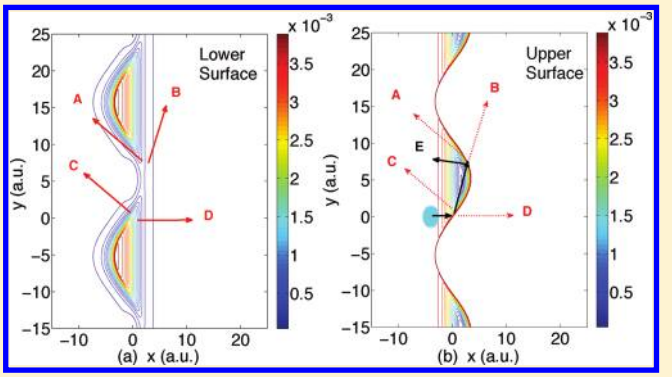

I. INTRODUCTION: FSSH AND DECOHERENCE

The fewest-switches surface-hopping (FSSH)[3,4] algorithm is one of the simplest and most widely applied nonadiabatic dynamics algorithms. The essence of the algorithm is to treat electrons quantum mechanically and nuclei classically, the latter moving according to Newton's laws on adiabatic surfaces. For reliable results, FSSH dictates that one propagate a swarm of classical particles, and transitions between electronic states occur with the smallest possible frequency in order to maintain consistency between the electronic amplitudes of each particle and the statistical distribution of different particles on the different adiabatic surfaces. When transitions between electronic states do occur, they are accompanied by velocity rescalings, i.e., discontinuities in the nuclear trajectories. As a straightforward nonadiabatic tool, FSSH has two key strengths: (i) FSSH propagates nuclei along strictly adiabatic surfaces rather than a mean field, so that one can model bond-making and -breaking events where using the correct asymptotic surface is crucial; (ii) FSSH forbids classical nuclei from populating energetically inaccessible electronic states, thereby closing all energetically forbidden channels during inelastic scattering and also approximately enforcing detailed balance.[5]

Despite its many strengths, the FSSH algorithm suffers one very well-known deficiency: overcoherence. This problem arises as follows. According to the FSSH algorithm, the electronic wave function is propagated exactly along a particular (stochastic) nuclear trajectory. As a result, components of the electronic wave function on different electronic surfaces always remain coherent (i.e., in phase) and each trajectory has an infinite memory of its past. Thus, even when a swarm of trajectories bifurcates between different adiabatic surfaces, each individual trajectory is unaware of the swarm's bifurcation and there is never a notion of independently propagated daughter wavepackets (as would be found with exact dynamics or multiple spawning[6,7]). Because of this limitation, one can find spurious FSSH results for long-time dynamics,[8] especially if nuclei visit more than one distinct region of derivative coupling.[1] Averaging FSSH trajectories over initial conditions does not remove the unphysical effects of overcoherence.[9]

To date, there is a relatively large body of literature for overcoming this decoherence problem while retaining a simple trajectory-based algorithm. During the 1990s, Rossky, Friesner, Prezhdo, and co-workers proposed adding decoherence directly and empirically to FSSH via stochastic wave function collapse.[10−16] Just as nuclear trajectories always have discontinuities in the usual FSSH algorithm, now electronic amplitudes should also behave discontinuously. These ideas were later expanded upon by Hammes-Schiffer[17] and Truhlar.[18−23] Schwartz and co-workers[24,25] and the present author[26] have considered wave function collapse on top of Ehrenfest (or mean-field) dynamics. Interestingly, surface-hopping algorithms that are independent from FSSH (and instead are derived from the quantum Liouville equation [QLE]) have been developed by Kapral and others.[27−38] QLE methods account for decoherence by allowing for steps in the density matrix where coherences propagate on the arithmetic average of two adiabatic surfaces, leading to a new phase

Received: July 11, 2011
Revised: September 19, 2011
Published: October 13, 2011

ACS Publications © 2011 American Chemical Society

and (on average) decoherence. All of the methods above have attractive features to them.

Recently, with Shenvi and Yang, we introduced two new algorithms for incorporating decoherence directly into the surface-hopping FSSH algorithm: (i) simultaneous trajectory surface hopping (STSH)[39] and (ii) augmented fewest-switches surface hopping (A-FSSH).[1] Both algorithms collapse the electronic wave function during an FSSH trajectory in order to account for wave packet separation on different surfaces but with novel approaches for determining a collapsing rate. Most importantly, these methods are free of any parametrization or fitting. On one hand, the STSH algorithm develops a decoherence rate based on the initial width of the wave packet at time zero.[39] On the other hand, A-FSSH assumes that, as a classical particle bifurcates on different potential energy surfaces, one can define an "intrinsic" width so that the collapse rate becomes roughly the difference in potential energy between the emerging wave packets divided by $\hbar$. The A-FSSH algorithm calculates the position centers for the virtual wave packets moving on different surfaces using a moment expansion of the Liouville equations (borrowing from Horsfield et al.[40−42]). As such, the A-FSSH algorithm is able to avoid the spawning problem in nonadiabatic dynamics.[43]

In this article, we will focus on the A-FSSH algorithm[1] as a means to correct traditional FSSH dynamics. In a future paper, we will compare A-FSSH and STSH dynamics. The goals of this paper are as follows: (i) we will now extend A-FSSH to arbitrarily many electronic states, whereas before we treated only two electronic states,[1] (ii) in order to ensure compatibility with the A-FSSH algorithm, we will rederive (and then implement) Shenvi's phase correction[2] for the electronic amplitude starting from the QLE, and (iii) we will rigorously examine a new two-dimensional model problem where we can quantify the effects of decoherence in a multidimensional context, investigating not just electronic populations (i.e., branching ratios) but also nuclear position and momentum distributions.

This article is arranged as follows. First, in section II, we review the theory and assumptions behind the original A-FSSH algorithm and discuss how the method can be extended to a general method with more than two electronic states. In this context, we also introduce the phase correction of Shenvi and co-workers. Most importantly, at the end of this section we give a concrete outline of how to perform A-FSSH dynamics step by step. Second, in section III, we present three new model Hamiltonians for quantifying decoherence and evaluating the different algorithms for numerical accuracy. We discuss and further interpret our results in section IV before concluding in section V.

A word about notation and constants. In what follows, electronic states are denoted by Roman letters, i, j, k, l,..., and we let N be the total number of electronic states. Nuclear coordinates are labeled by Greek characters, α, β, γ,... Electronic operators are denoted with superscript hats, and nuclear operators are denoted by bold characters. In particular, $\hat{r}$ is the position operator for an electron and $\boldsymbol{R}$ is the position operator for a nucleus. The electronic Hamiltonian is written as $\hat{V}$, adiabatic electronic states are labeled $|\Phi_i(r;R)\rangle$, and the derivative couplings are $d_{ij}^{\alpha} = \langle\Phi_i|(\partial/(\partial R^{\alpha}))\Phi_j\rangle$. In the numerical section, all particles are chosen to have mass $m = 2000$ au.

II. AUGMENTED AND PHASE-CORRECTED FSSH

II.A. Review: Moment Expansions, Decoherence, and a Phase Correction. The decoherence criterion in the A-FSSH algorithm is based upon a moment expansion in phase space, a Gaussian ansatz, and an optimal width conjecture. We now outline briefly all steps needed for recovering a decoherence rate.

II.A.1. Choice of Moments. Borrowing from the correlated electronic-ionic dynamics (CEID) of Horsfield, Bowler, Todorov, and co-workers,[40−42] the A-FSSH algorithm propagates the first moments of position and momentum relative to some specified trajectory. Here, we choose that specified trajectory to be a Tully style[3] FSSH trajectory, $(R_{SH}(t),P_{SH}(t))$. In terms of the exact total (nuclear plus electronic) density matrix, $\hat{\boldsymbol{\rho}}(t) = |\psi(t)\rangle\langle\psi(t)|$, these moments are defined by

$$\hat{\sigma}(t) \equiv \mathrm{Tr}_N(\hat{\boldsymbol{\rho}}(t)) \tag{1}$$

$$\delta\hat{R}^{\alpha}(t) \equiv \mathrm{Tr}_N(\delta\mathbf{R}^{\alpha}\hat{\boldsymbol{\rho}}(t)) \equiv \mathrm{Tr}_N((\mathbf{R}^{\alpha}(t) - R_{SH}^{\alpha}(t))\hat{\boldsymbol{\rho}}(t)) \tag{2}$$

$$\delta\hat{P}^{\alpha}(t) \equiv \mathrm{Tr}_N(\delta\mathbf{P}^{\alpha}\hat{\boldsymbol{\rho}}(t)) \equiv \mathrm{Tr}_N((\mathbf{P}^{\alpha}(t) - P_{SH}^{\alpha}(t))\hat{\boldsymbol{\rho}}(t)) \tag{3}$$

II.A.2. Equations of Motion for the Moments. In order to propagate these moments forward in time, we expand the full time-dependent Liouville equation for the full nuclear-electronic density matrix about an FSSH trajectory and throw away all second- and higher-order terms (plus all second derivatives of the potential energy, $\hat{K}^{\alpha\beta}$). The result is

$$\frac{\mathrm{d}}{\mathrm{d}t}\delta R_{jk}^{\alpha} = \frac{-i}{\hbar}[\hat{V},\delta\hat{R}^{\alpha}]_{jk} + \frac{\delta P_{jk}^{\alpha}}{M^{\alpha}} - \sum_{\beta}\frac{P_{SH}^{\beta}}{M^{\beta}}[\hat{d}^{\beta},\delta\hat{R}^{\alpha}]_{jk} \tag{4}$$

$$\frac{d}{dt}\delta P_{jk}^{\alpha} = \frac{-i}{\hbar}[\hat{V},\delta\hat{P}^{\alpha}]_{jk} + \frac{1}{2}(\delta\hat{F}^{\alpha}\hat{\sigma} + \hat{\sigma}\delta\hat{F}^{\alpha})_{jk} - \sum_{\beta}\frac{P_{SH}^{\beta}}{M^{\beta}}[\hat{d}^{\beta},\delta\hat{P}^{\alpha}]_{jk} \tag{5}$$

where $\hat{V} \equiv \hat{V}(\vec{R}_{SH}(t))$ is the potential energy matrix and $\hat{F}^{\alpha} \equiv \hat{F}^{\alpha}(\vec{R}_{SH}(t)) = -(\partial\hat{V})/(\partial R^{\alpha})$ is the force matrix. We define $\delta\hat{F}^{\alpha} \equiv \hat{F}^{\alpha} - F_{SH}^{\alpha}$, where F_{SH}^{α} is the force on the active surface at position $\vec{R}_{SH}$.

II.A.3. Exact Decoherence Rate from the Liouville Equation. When expanding the Liouville equation above, we find that the equation of motion for $\hat{\sigma}$ is not exactly the standard time-dependent electronic Schrodinger equation (TDSE), i.e., the electronic density matrix is no longer just a slave to the nuclear coordinates (see eq 14). Instead, what emerges is a more complicated expression with a simple and natural rate of decoherence between wave packets on surfaces i and j, assuming we are in a region of configuration space where $d_{ij}^{\alpha} = 0$.

In order to see this result, we define matrix elements for the standard electronic density matrix in eq 1 above

$$\sigma_{jk}(t) \equiv \langle\Phi_j(\vec{R}_{SH})|\mathrm{Tr}_N(\hat{\boldsymbol{\rho}}(t))|\Phi_k(\vec{R}_{SH})\rangle = \int dR'\langle\Phi_j(\vec{R}_{SH})R'|\hat{\boldsymbol{\rho}}(t)|\Phi_k(\vec{R}_{SH})R'\rangle \tag{6}$$

Taking the time derivative of eq 6 and using the Liouville equation, $(\partial/\partial t)\hat{\boldsymbol{\rho}} = (-i/\hbar)[\hat{\mathbf{H}}, \hat{\boldsymbol{\rho}}]$, we find

$$\frac{\mathrm{d}}{\mathrm{d}t}\sigma_{jk}(t) = -\frac{i}{\hbar}\int \mathrm{d}R' \langle \Phi_j R'|[\hat{\mathbf{H}}, \hat{\boldsymbol{\rho}}]|\Phi_k R'\rangle + \int \mathrm{d}R' \left\langle \frac{\mathrm{d}\Phi_j}{\mathrm{d}t} R'|\hat{\boldsymbol{\rho}}(t)|\Phi_k R'\right\rangle + \int \mathrm{d}R' \left\langle \Phi_j R'|\hat{\boldsymbol{\rho}}(t)|\frac{\mathrm{d}\Phi_k}{\mathrm{d}t} R'\right\rangle \tag{7}$$

$$= -\frac{i}{\hbar}\int \mathrm{d}P' \langle \Phi_j P'|[\mathbf{T}, \hat{\boldsymbol{\rho}}]|\Phi_k P'\rangle - \frac{i}{\hbar}\int \mathrm{d}R' \langle \Phi_j R'|[\hat{\mathbf{V}}, \hat{\boldsymbol{\rho}}]|\Phi_k R'\rangle + \sum_\alpha \frac{\mathrm{d}R^\alpha_{SH}}{\mathrm{d}t}\left(\int \mathrm{d}R' \left\langle \frac{\partial \Phi_j}{\partial R^\alpha_{SH}} R'|\hat{\boldsymbol{\rho}}(t)|\Phi_k R'\right\rangle + \int \mathrm{d}R' \left\langle \Phi_j R'|\hat{\boldsymbol{\rho}}(t)|\frac{\partial \Phi_k}{\partial R^\alpha_{SH}} R'\right\rangle\right) \tag{8}$$

$$= -\frac{i}{\hbar}\int \mathrm{d}R' \langle \Phi_j R'|[\hat{\mathbf{V}}, \hat{\boldsymbol{\rho}}]|\Phi_k R'\rangle - \sum_\alpha \frac{P^\alpha_{SH}}{M^\alpha}[\hat{d}^\alpha, \hat{\sigma}]_{jk} \tag{9}$$

Expanding the potential around $\vec{R}_{SH}(t)$

$$\hat{\mathbf{V}} = \hat{V}(\vec{R}_{SH}) - \sum_\alpha \hat{F}^\alpha(\vec{R}_{SH})(\delta \boldsymbol{R}^\alpha) + \sum_{\alpha,\beta} \hat{K}^{\alpha\beta}(\vec{R}_{SH})(\delta \boldsymbol{R}^\alpha \delta \boldsymbol{R}^\beta) + \ldots \tag{10}$$

we find

$$\frac{\mathrm{d}}{\mathrm{d}t}\sigma_{jk}(t) = -\frac{i}{\hbar}[\hat{V}, \hat{\sigma}]_{jk} + \sum_\alpha \frac{i}{\hbar}[\hat{F}^\alpha, \delta\hat{R}^\alpha]_{jk} - \sum_\alpha \frac{P^\alpha_{SH}}{M^\alpha}[\hat{d}^\alpha, \hat{\sigma}]_{jk} + \ldots \tag{11}$$

From eq 11, we see that the TDSE is correct only to zeroth order; there is also a first-order correction term, $[\hat{F}^\alpha, \delta\hat{R}^\alpha]$, and this term cannot be incorporated into the Hamiltonian. Interestingly, *if we assume that we are in a region with zero derivative couplings* $d^\alpha_{ij} = 0$, this term leads to a decoherence rate with a simple form

$$\frac{1}{\tau^{ij}_d} = -\frac{\frac{\mathrm{d}}{\mathrm{d}t}|\sigma_{ij}(t)|}{|\sigma_{ij}(t)|} = -\frac{\frac{\mathrm{d}}{\mathrm{d}t}|\sigma_{ij}(t)|^2}{2|\sigma_{ij}(t)|^2} = \mathrm{Im}\sum_\alpha \left(\frac{(F^\alpha_{ii} - F^\alpha_{jj})\delta R^\alpha_{ij}}{\hbar \sigma_{ij}}\right) \tag{12}$$

Lastly, we have seen that eq 11 leads to a mixed density matrix that cannot be reduced to a single equation of motion for the electronic amplitude. Note that if we throw away the $[\hat{F}, \delta\hat{R}]$ term we recover the standard time-dependent Schrodinger equation (TDSE)

$$\frac{\mathrm{d}}{\mathrm{d}t}\sigma_{jk}(t) = -\frac{i}{\hbar}[\hat{V}, \hat{\sigma}]_{jk} - \sum_\alpha \frac{P^\alpha}{M^\alpha}[\hat{d}^\alpha, \hat{\sigma}]_{jk} \tag{13}$$

or, equivalently, for the amplitude $\vec{c}$ (where $\sigma_{ij} = c_i c_j^*$)

$$\frac{\mathrm{d}c_j}{\mathrm{d}t} = -\frac{i}{\hbar}\sum_k V_{jk}c_k - \sum_{k\alpha}\frac{P^\alpha}{M_\alpha} d^\alpha_{jk} c_k \tag{14}$$

II.A.4. Shenvi Phase Correction. On the basis of Heller's frozen Gaussian dynamics, Shenvi recently suggested[2] replacing the usual TDSE in eq 14 by eq 15

$$\frac{\mathrm{d}}{\mathrm{d}t}c_j(t) = \frac{i}{\hbar}\sum_\alpha \frac{P^\alpha_{SH}P^\alpha_j}{M^\alpha} c_j - \sum_{\alpha,k}\frac{P^\alpha_{SH}}{M^\alpha}\hat{d}^\alpha_{jk}c_k + \ldots \tag{15}$$

Equation 15 requires different momenta for each adiabatic electronic surface. While the magnitude of each momentum can be assigned by energy conservation, the direction of momentum on each surface is not well defined for all but the active surface. Following ref 2 we will make the assumption of "parallel momenta", so that all momenta are chosen in the same direction as the particle's active momentum. If surface i is the active surface this implies

$$\vec{P}_j = \eta \vec{P}_i \quad \eta \geq 0 \tag{16}$$

where η is fixed by energy conservation

$$E_{\mathrm{tot}} = \sum_\alpha \frac{(P^\alpha_j)^2}{2M^\alpha} + V_{jj}(\vec{R}_{SH}) = \sum_\alpha \frac{(P^\alpha_i)^2}{2M^\alpha} + V_{ii}(\vec{R}_{SH}) \tag{17}$$

In the Appendix, we will rederive this result starting from the quantum Liouville equation with a host of approximations: (i) a frozen Gaussian ansatz, (ii) negligible zero-point energy, (iii) zero position moments $\delta\hat{R} = 0$, and (iv) a rough extraction of a pure state from a mixed density matrix. With these approximations, eq 15 is correct to first order. Recall, though, that the usual TDSE is also correct to first order if we assume that $\delta\hat{R} = 0$, see eq 11. In practice, however, we will show below that, for one-dimensional systems in particular, this phase-corrected TDSE (eq 15) leads to much improved results relative to the usual TDSE (eq 14).

II.A.5. Gaussian Ansatz and Optimal Width Conjecture. A well-defined and stable decoherence rate based on eq 12 can be found by modeling the system as a sum of frozen Gaussian nuclear wave packets, each multiplied by an adiabatic electronic state $\Phi_j(r;R)$

$$\langle \vec{r}, \vec{R}\,|\Psi(t)\rangle \approx \sum_j c_j g_j(\vec{R})\Phi_j(\vec{r};\vec{R}) \tag{18}$$

$$g_i(\vec{R}) \equiv \left\langle \vec{R}\,|g_i(\vec{R}_i(t), \vec{P}_i(t))\right\rangle \tag{19}$$

$$\equiv \prod_\alpha \left(\frac{1}{\pi a^2_{R^\alpha}}\right)^{1/4} \exp\left(\frac{-(R^\alpha - R^\alpha_i(t))^2}{2a^2_{R^\alpha}}\right) \times \exp\left(\frac{i}{\hbar}P^\alpha_i(t)(R^\alpha - R^\alpha_i(t))\right) \tag{20}$$

This allows us to estimate $\mathrm{Im}(\delta R^\alpha_{ij}/\sigma_{ij}) = (P^\alpha_i - P^\alpha_j)a^2_{R^\alpha}/(2\hbar)$. We next make an optimal width conjecture; namely, we assume that

the width of the Gaussian wave packet on each surface adjusts so as to maximize overlap with wave packets on other surfaces $(\partial/(\partial a_R^\alpha))|\langle g_i|g_j\rangle| = 0$. This leads to the following estimate of the width of the nuclear wave packets

$$a_{R^\alpha}^2 = \hbar \frac{|R_i^\alpha - R_j^\alpha|}{|P_i^\alpha - P_j^\alpha|} \tag{21}$$

and plugging into eq 12 an approximate lower bound for the decoherence rate between wave packets on surfaces i and j

$$\frac{1}{\tau_d^{ij}} \approx \sum_\alpha \left(\frac{(F_{ii}^\alpha - F_{jj}^\alpha)(\delta R_{ii}^\alpha - \delta R_{jj}^\alpha)}{2\hbar} \right) \Theta[(\delta R_{ii}^\alpha - \delta R_{jj}^\alpha)(\delta P_{ii}^\alpha - \delta P_{jj}^\alpha)] \tag{22}$$

Here, the Heaviside function Θ has been introduced, so that decoherence in the α direction is positive only when $\delta R_{ii}^\alpha - \delta R_{jj}^\alpha$ and $\delta P_{ii}^\alpha - \delta P_{jj}^\alpha$ have the same sign.

II.A.6. Regions with Non-Negligible Derivative Coupling. Because eq 12 is strictly valid only in regions where $d_{ij}^\alpha = 0$, it follows that eq 22 is also valid only if the derivative couplings vanishes. As such, eq 22 ignores the quantum fluctuations in energy caused by state mixing and the cross terms in eq 11 caused by d_{ij}^α. To correct for this failure and to be sure that we do not overestimate decoherence, we will empirically modify this decoherence rate so that forces in opposite directions on the adiabatic surfaces must overcome the quantum force $\vec{F}_{ij}$

$$Z_{ni}^\alpha \equiv \frac{(F_{nn}^\alpha - F_{ii}^\alpha)(\delta R_{nn}^\alpha - \delta R_{ii}^\alpha) - |F_{in}^\alpha||\delta R_{nn}^\alpha - \delta R_{ii}^\alpha|}{2\hbar} \tag{23}$$

$$\frac{1}{\tau_d^{ni}} = \sum_\alpha Z_{ni}^\alpha \Theta(Z_{ni}^\alpha) \Theta[(\delta R_{nn}^\alpha - \delta R_{ii}^\alpha)(\delta P_{nn}^\alpha - \delta P_{ii}^\alpha)] \tag{24}$$

Equation 24 is the final decoherence rate as implemented in our algorithm. In these equations, we choose to estimate the intrinsic quantum fluctutations between surfaces i and n by $(F_{in}^\alpha(\delta R_{nn}^\alpha - \delta R_{ii}^\alpha))/(2\hbar)$ because this very expression appears in eq 11 when $\vec{F}_{in}\vec{d}_{in} \neq 0$. By incorporating this fluctuation term into our decoherence rate and insisting that wave packets must overcome this barrier before separation, we do not usually decohere our quantum system at the avoided crossing; instead, we enforce decoherence just after the avoided crossing and only when the different surfaces and forces do really lead to long-time wave packet separation. Moreover, in practice, we find that including this quantum fluctuation term prevents the algorithm from implementing too many collapsing events. Note that eqs 23 and 24 are new to this article and were not implemented previously in ref 1.

II.B. Decoherence Beyond Two Electronic States. The ideas above give us a natural approach for implementing decoherence on top of FSSH trajectories, and the algorithm has already been implemented successfully for two electronic states.[1] When extending the A-FSSH algorithm to more than two electronic states, however, new questions arise. In particular: (i) how do we treat the position and momentum moments after a collapsing event and (ii) how do we treat these moments after a hopping event between surfaces? For the case of only two electronic states, empirically we find that these questions are not extremely important as almost all protocols lead to similar answers. With multiple electronic states, however, we can find nonsensical results if we are not careful. For instance, suppose a particle hops from surface 1 to 2 but all the while there is a nonzero amplitude on surface 3. Should we maintain coherence of the moments after a hop or not? Without careful attention, we can find completely incorrect dynamics as caused by faulty treatments of the moments. Having considered several different possible answers for the questions above, both theoretically and practically, we offer solutions to these problems in the Appendix.

II.C. Step-by-Step Algorithm. In order to be as clear as possible, we now outline our extended algorithm for incorporating decoherence into traditional FSSH dynamics with multiple electronic states. A step-by-step outline of our algorithm is as follows.

1 As in standard FSSH, we initialize the mixed quantum-classical trajectory by fixing the initial classical coordinates $\vec{R}_0, \vec{P}_0$ and electronic amplitude $\vec{c}_0$ at time $t = 0$. For simplicity, we assume our dynamics begin on a single adiabatic electronic state (say, i), so we set $\vec{c} = |i\rangle$. We also set $\delta\hat{R} = \delta\hat{P} = 0$.

2 Between time t and $t + dt$, we propagate our dynamical variables.

(a) For nuclear coordinates, as in standard FSSH, we propagate $\vec{R}, \vec{P}$ according to Newton's laws

$$\frac{dR^\alpha}{dt} = \frac{P^\alpha}{M} \tag{25}$$

$$\frac{dP^\alpha}{dt} = F_{ii}^\alpha(\vec{R}) \tag{26}$$

(b) For the electronic amplitude, if we are running standard A-FSSH, we propagate $\vec{c}$ according to eq 14 (the standard TDSE). If we are running phase-corrected A-FSSH, we propagate $\vec{c}$ according to eqs 15−17, where now the active surface i is crucial.

(c) Unique to A-FSSH, we propagate the moments $\delta\hat{R}$ and $\delta\hat{P}$ according to eqs 4 and 5, respectively.

3 As in standard FSSH, while the nuclei are being propagated along the ith adiabatic electronic surface, at each time step we evaluate the probability to hop to any other state (labeled $j \neq i$, for instance), $\gamma_{\text{hop}}^{i\to j}$. This hopping probability is chosen to be as small possible while still forcing the relative populations on different surfaces to match the norm of the electronic amplitudes. It can be shown[3] in a straightforward manner that in a simulation time step dt this probability is

$$\gamma_{\text{hop}}^{i\to j} = -\sum_\alpha \frac{2P^\alpha}{M^\alpha} \frac{\text{Re}(d_{ji}^\alpha(\vec{R})\sigma_{ij})}{\sigma_{ii}} dt \tag{27}$$

As in standard FSSH, in order to implement the probabilities above, we use a random number generator to construct a random number $\zeta \in [0,1]$. The total rate of hopping is $\gamma_{\text{tot}} = \Sigma_j \gamma_{\text{hop}}^{i\to j}$ and these rates are added together into one big array

$$S_j = \sum_{l\le j} \gamma_{\text{hop}}^{i\to l} \tag{28}$$

Here, we define $S_0 \equiv 0$, and it is easy to see that $S_N = \gamma_{\text{tot}}$. Also, because we set $\gamma_{\text{hop}}^{i\to i} = 0$, clearly $S_i = S_{i-1}$.

(a) If $\zeta > \gamma_{\text{tot}}$, do not hop. Continue to step 6.

(b) If $\zeta < \gamma_{\text{tot}}$, then provided the hop is energetically allowed there will be a hopping event to surface j, where $S_{j-1} < \zeta < S_j$. Continue to step 4.

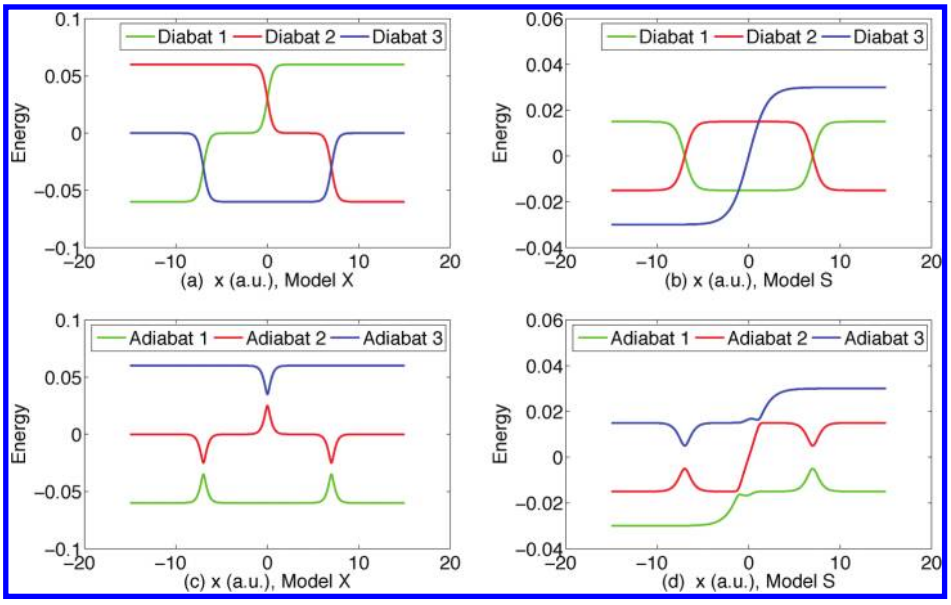

Figure 1. Diabatic and adiabatic potential energy curves for the models with three electronic states described in eqs 33 (model X, left) and 34 (model S, right).

4 As in standard FSSH, in order to maintain energy conservation when moving from the *i*th to the *j*th adiabatic potential energy surface, we compute a rescaled nuclear momentum in a direction $\vec{u}_{sc}$, chosen to be the direction of derivative coupling ($\vec{u}_{sc} = \vec{d}_{ij}$)

$$\vec{P}^{\text{new}} = \vec{P} + \kappa \vec{u}_{sc} \tag{29}$$

$$\sum_{\alpha} \frac{(P^{\alpha,\text{new}} \cdot u_{sc}^{\alpha})^2}{2M^{\alpha}} + V_{jj}(\vec{R}) = \sum_{\alpha} \frac{(P^{\alpha} \cdot \vec{u}_{sc})^2}{2M^{\alpha}} + V_{ii}(\vec{R}) \tag{30}$$

Equation 30 gives a quadratic equation for κ with two possible roots; we choose the root with smallest $|\kappa|$. We will discuss other choices of rescaling direction ($\vec{u}_{sc}$) in section IV.

(a) If the upper state is not accessible, continue to step 6.
(b) If the upper state is accessible (and, thus, $\vec{P}^{\text{new}}$ is real), a hop occurs. Continue to step 5

5 Given that a hop will now occur, we must adjust all our variables.
(a) Rescale the momentum, $\vec{P} = \vec{P}^{\text{new}}$ according to eq 30.
(b) Following the protocol in the Appendix, translate the position moments ($\delta\vec{R}$) according to eqs 44 and 45.
(c) Translate the momentum moments ($\delta\vec{P}$) according to eqs 46−48.
(d) If the diagonal momentum moment on any surface *n* cannot be adjusted so as to conform to eq 48, i.e., $\delta\vec{P}^{\alpha}_{nn}$ is now imaginary for some α, we implement a decoherence event as in eq 32.
(e) Switch the labels of electronic surfaces *i* and *j* (so that we are again walking on the "*i*th" surface) and continue to step 6.

6 For each electronic amplitude $n \neq i$, we construct the probability for decoherence in the time interval d*t* (and separation from the nuclear wave packet on the active [*i*th] adiabatic electronic state) by evaluating

$$\gamma_n^{\text{collapse}} = \text{d}t \frac{1}{\tau_d^{ni}} \tag{31}$$

where d*t* is the simulation time step and $1/\tau_d^{ni}$ is defined in eqs 23 and 24.

(a) Loop over *n*.
i For each state $n \neq i$, we generate a random number, $\eta_n \in [0,1]$.
ii If $\eta_n > \gamma_n^{\text{collapse}}$, there is no collapsing event.
iii If $\eta_n < \gamma_n^{\text{collapse}}$, there is a collapsing event and the component of the electronic amplitude on state *n* vanishes. The electronic amplitudes are collapsed according to eq 32.

$$c_j^{\text{new}} = \begin{cases} c_j/\eta & j \neq n \\ 0 & j = n \end{cases} \qquad \eta = \sqrt{1 - \sum_{l \neq n} |c_l|^2} \tag{32}$$

End loop over *n*.
(b) If a collapsing event has occurred for any of the surfaces, we follow the protocol in the Appendix, so that the position and momentum moments are rescaled according to eqs 41 and 42.
(c) Return to step 2.

In step 6 above, the premise is that as we follow the active wave packet on surface *i*, we check whether all other wave packets on different inactive surfaces *n* are moving away relative to us. For each such wavepacket (say, on surface *n*) there is a finite probability for separation or, more precisely, loss of coherence with the active wave packet; to allow all such possibilities, we must loop over *n* in step 6a. Using this intuition we can now treat the case where either single or multiple wave packets are decohered.

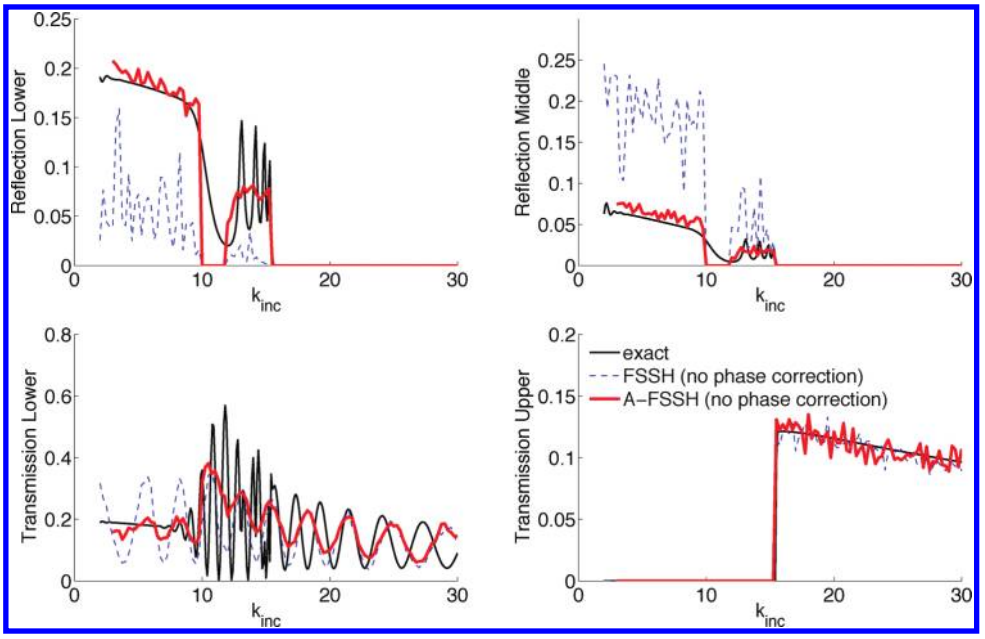

Figure 2. Branching ratios for the Hamiltonian in eq 33 (which is plotted in Figure 1a and 1c) as a function of the incoming momentum k_{inc}. The particle starts originally on the middle adiabatic surface, and all surface-hopping values are averaged over 2000 trajectories. Here, all results are for FSSH algorithms using the standard TDSE (eq 14). We assume the incoming particle has a well-defined momentum (a plane wave for the exact calculations), and we do not average over any spread in momentum for the surface-hopping results.

At the same time, note that the expressions in eqs 31, 23, and 24 depend only on two states—one active, the other inactive—and the matrix elements of $\hat{F}$, $\delta\hat{R}$ between them. Thus, the instantaneous probability for one state m to vanish by collapse is independent of the probability for any other state n to vanish by collapse and the ordering of the electronic states is, of course, irrelevant.

III. NUMERICAL RESULTS

We now present three numerical studies to test the algorithm presented above. First, we treat two different potentials each with three electronic states and one nuclear dimension. Then, for a carefully chosen problem of two electronic states in two nuclear dimensions, we examine the effect of decoherence on both branching ratios and position/momentum distributions. All calculations were carried out with a Runge−Kutta 4/5 integrator and a time step of $dt = 0.3$ au.

III.A. Three Electronic States. We describe below two potentials with one nuclear dimension and three electronic states, labeled model X and model S. These models have several avoided crossing and, as such, are challenging models for any surface-hopping scheme.

III.A.1. Model X. For our first model problem, we choose a diabatic Hamiltonian of the form

$$\begin{aligned} V_{11} &= A(\tanh(Bx) + \tanh(B(x+7))) \\ V_{22} &= -A(\tanh(Bx) + \tanh(B(x-7))) \\ V_{33} &= -A(\tanh(B(x+7)) - \tanh(B(x-7))) \\ V_{12} &= C\exp(-(x^2)) \\ V_{13} &= C\exp(-(x+7)^2) \\ V_{23} &= C\exp(-(x-7)^2) \end{aligned} \tag{33}$$

where we choose $A = 0.03$, $B = 1.6$, and $C = 0.005$, all in atomic units. The diabatic and adiabatic curves for model X are shown in Figure 1.

We imagine a particle entering from the left on the second adiabatic electronic surface. For incoming momenta $k_{inc} < 15$ au the particle does not have enough kinetic energy to emerge on the highest excited state and any wave packet that attempts to do so will be reflected. The result is that decoherence is important: below an energy threshold $k_{inc} < 15$ au, the parent wave packet will break apart into transmitted and reflected daughters.

In many ways, model X is similar to the Hamiltonian in ref 9. In both cases, wave packets on two different surfaces must separate when they feel different forces. The essential and difficult new twist is, however, that we now include three electronic states. In particular, before the avoided crossing near $x = 0$, the particle has already gone through another avoided crossing near $x = -7$. Thus, when the second avoided crossing happens between adiabats 2 and 3, there can now be three nonzero electronic amplitudes. The next question becomes, of course, when the wave packets moving on the middle and upper surfaces decohere, what are the implications for the electronic amplitude on the lower surface? Does it stay coherent with one of the wave packets? Does it decohere from both amplitudes?

Our results are shown in Figures 2 and 3. In these figures, we plot branching ratios for incoming plane waves with a well-defined momentum (and infinite width in position space). There are three energy regimes. For $k_{inc} < 9$, the incoming wave packet does not have enough energy to climb over the barrier on the adiabatic middle surface. For $9 < k_{inc} < 12$, the upper surface can be populated only near $x = 0$, not asymptotically. For $k_{inc} > 15$, the upper channel is opened for good. In Figure 2, we plot results where the electronic amplitude is propagated with the standard TDSE. In Figure 3, we show results using the phase correction of Shenvi and co-workers.[2]

From the figures, we see that decoherence is very important for this problem. Below $k_{inc} < 9$ there are no oscillations according to the exact branching ratios. By contrast, FSSH ratios consistently

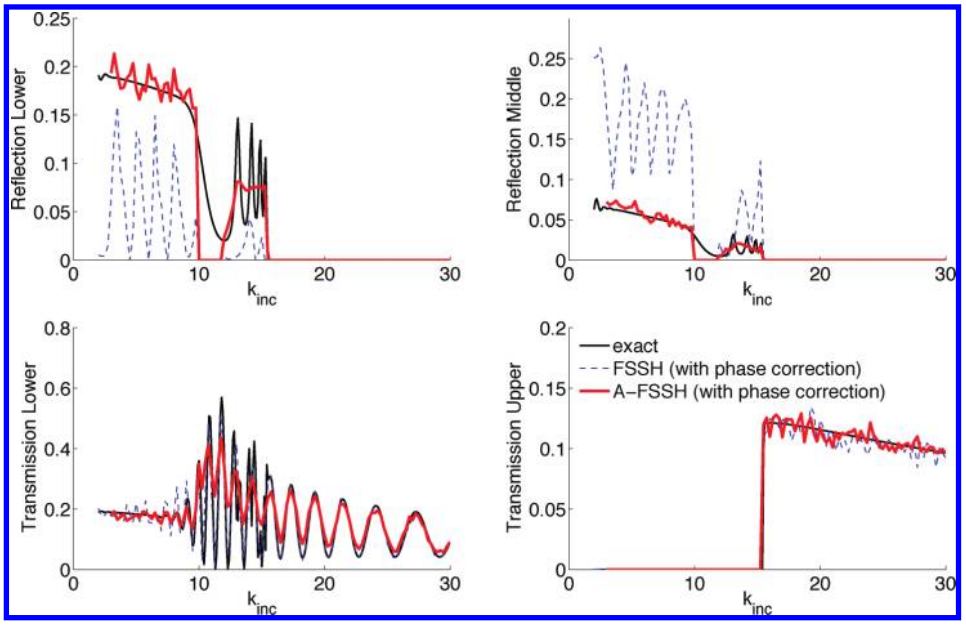

Figure 3. Same plots as in Figure 2, only now using the phase of correction of Shenvi and co-workers[2] (eq 15). Note the remarkable improvement in results when we both implement the phase correction and apply decoherence.

and incorrectly oscillate: the reflection and transmission branching ratios both oscillate because the trajectories recross at $x = \pm 7$. When we apply decoherence, the standard A-FSSH algorithm collapses almost all reflecting trajectories, so there are only very small oscillations in this energetic regime. The existence of small oscillations does suggest, however, that the algorithm has not provided quite enough decoherence. We reach the same conclusion looking at the transmission branching ratios at low energies, where we again see small oscillations. In particular, for a particle moving forward on the ground surface at $x = 0$, the electronic amplitude is not quite decohered from *both* of the upper surfaces. This represents a partial failure of the algorithm and the first-order moment expansion in eqs 1−5 as the potential energies here are changing rapidly.

In the energetic regime $9 < k_{inc} < 15$, we find the opposite problem. Now, a particle moving along the middle adiabatic surface can transmit over the barrier and have a recrossing event with the lower adiabatic surface. This leads to sharp oscillations in the branching ratios. As we see from Figure 2, A-FSSH predicts there should be a finite (nonzero) amount of decoherence at the avoided crossing between the upper and middle surfaces, and as a result, the final branching ratios are damped out (incorrectly). This is, however, not terribly surprising nor terribly problematic: these oscillations require wave packets that are extremely wide in position space (and narrow in momentum space), so that these wave packets are not very classical; therefore, all surface-hopping algorithms should fail. If we consider a wave packet with a finite width in position space, these very sharp oscillations in the exact branching ratios will be severely washed away as we average over plane wave branching ratios, as in ref 9.

Finally, at large incoming energies decoherence is no longer a concern and all particles transmit without any decoherence. In this energetic regime, A-FSSH and FSSH give identical results, neither very good as their oscillating branching ratios do not have the correct period or phase. With this in mind, one of the most interesting results in this paper is Figure 3. Here, we show numerical results when we implement the phase-corrected equation of motion for the electronic degrees of freedom (eq 15). One can see that we now recover effectively exact results at high energies! In this energy range, where decoherence is minimal, the phase correction correctly treats all processes with multiple hops between surfaces, representing a big improvement over the standard TDSE (eq 14).

In the end, these calculations are quite encouraging. At low energies, our recipe for decoherence leads to nearly the correct collapsing rate. The phase correction of Shenvi[2] is obviously crucial for solving this problem accurately, especially at high energies.

III.A.2. Model S. As a second model problem with three electronic degrees of freedom, we now investigate the following diabatic Hamiltonian (labeled Model S)

$$\begin{aligned} V_{11} &= A(\tanh(B(x-7)) - \tanh(B(x+7))) + A \\ V_{22} &= -A(\tanh(B(x-7)) - \tanh(B(x+7))) - A \\ V_{33} &= 2A\tanh(Dx) \\ V_{12} &= C\exp(-(x+7)^2) + C\exp(-(x-7)^2) \\ V_{13} &= C\exp(-x^2) \\ V_{23} &= C\exp(-x^2) \end{aligned} \tag{34}$$

Here we choose $A = 0.015$, $B = 1.0$,$C = 0.005$, and $D = 0.5$. The diabatic and adiabatic potentials are plotted in Figure 1. Again, we approach the interaction region from the left, coming in along the middle adiabatic electronic state.

Model S has many of the same features as Model X. For low energies, $k < 10$, the dynamics are simple: there is a large barrier before the particle leading to complete reflection on the middle surface. For high energies, $k > 14$, the dynamics are also straightforward, as there is no reflection, the particle always transmits, decoherence is minimal, and one must only integrate an electronic equation of motion. The most interesting decoherence dynamics are all in the range $10 < k < 14$ when a classical particle reflects on the upper surface near $x = 0$, now having already passed through two avoided crossings rather than one, as

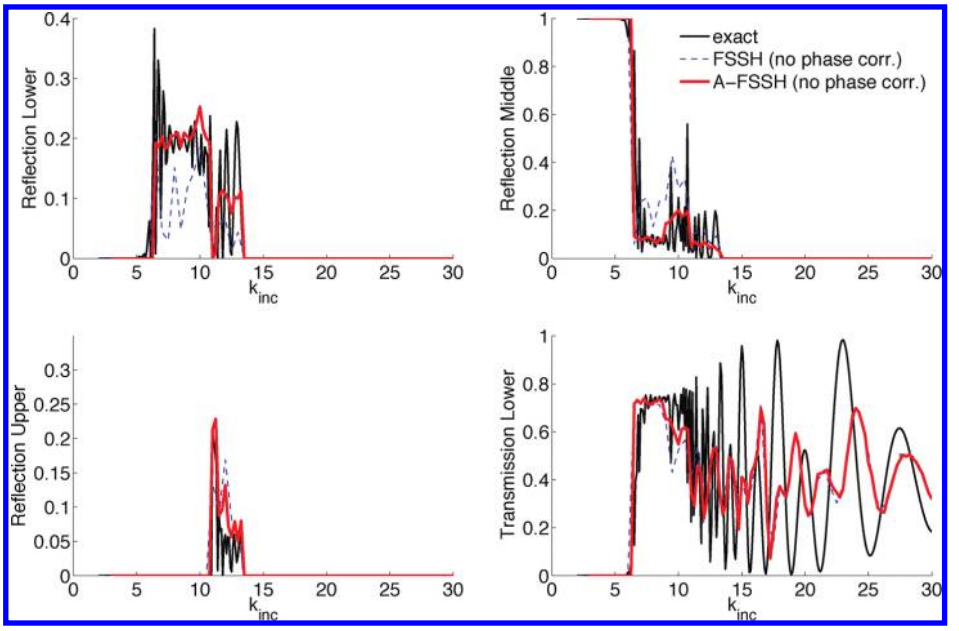

Figure 4. Branching ratios for the Hamiltonian in eq 34 (which is plotted in Figure 1b and 1d) as a function of the incoming momentum k_{inc}. The particle comes in from the left along the middle adiabatic surface, and all surface-hopping values are averaged over 2000 trajectories. Here, all results are for FSSH-based algorithms using the standard TDSE (eq 14). We assume the incoming particle has a well-defined momentum (a plane-wave for the exact calculations), and we do not average over any spread in momentum for the surface-hopping results.

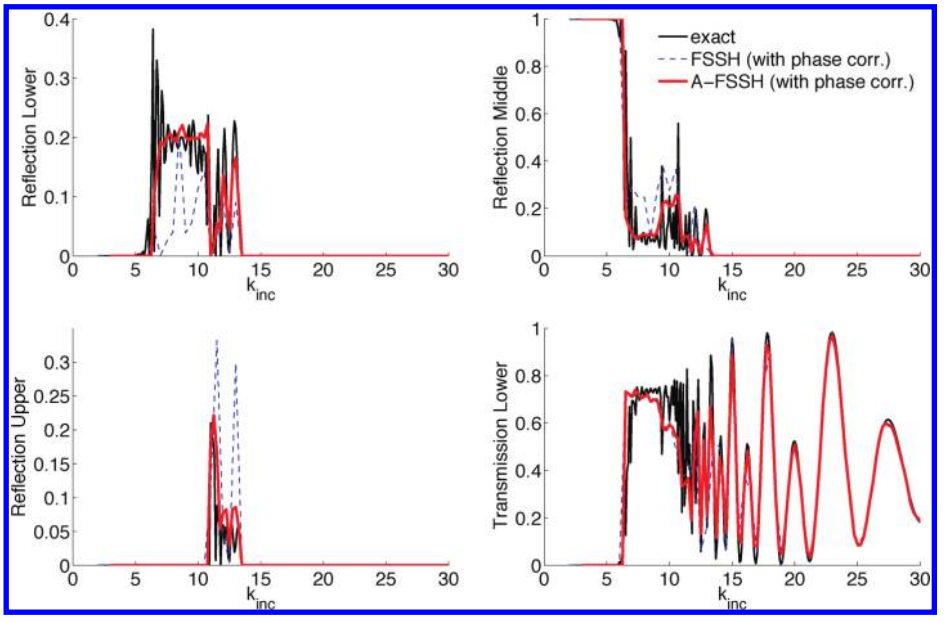

Figure 5. Same plots as in Figure 4, only now using the phase of correction of Shenvi and co-workers[2] (eq 15), which leads to much improved results.

in Model X. In this way, Model S is more complicated than Model X, and we expect to see extremely perverse branching ratios if decoherence is not implemented.

We plot our resuls in Figures 4 and 5. As we would expect, at low incoming kinetic energies, the results are greatly improved using the A-FSSH algorithm as compared to the standard FSSH routine because decoherence is crucial. However, just as for model X, the standard A-FSSH algorithm does not agree with exact results at high energy. At such high energies, decoherence is small and the phase correction of Shenvi and co-workers is essential for trajectories that hop more than once. The agreement between phase-corrected surface hopping and exact results at high energies in Figure 5 is quite remarkable.

For intermediate incoming energies, $10 < k < 14$, this model Hamiltonian becomes quite complicated. Here, there are extremely narrow quantum resonances that we cannot reproduce with a classical surface-hopping algorithm. As for model X, however, these resonances will disappear after averaging over the width of a classical particle. With this in mind, we see that the standard A-FSSH algorithm does fairly well in this regime: we keep some of the resonance features while washing away others. In particular, for reflection branching ratios, A-FSSH continues

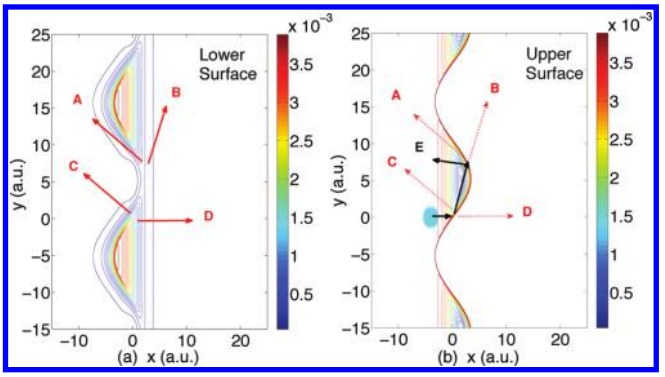

Figure 6. Potential energy contours for the lower (a) and upper (b) adiabatic surfaces for the Hamiltonian in eq 35. Here, we imagine starting a particle as a Gaussian wave packet on the upper surface (shown in blue in b), and this particle spawns fragments C−D (first) and A−B (second) on the lower surface. Fragment E represents the remaining packet on the upper adiabatic surface at the end of all scattering events.

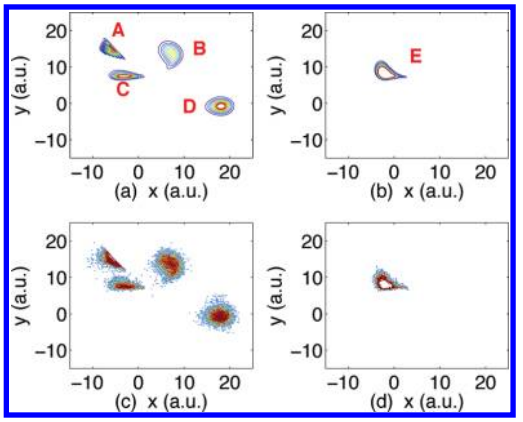

Figure 7. (a and b): Positional distribution of a quantum wave packet propagated exactly using a grid at time t = 2300 au. The wave packet starts at $(x,y) = (-4,0)$ with $\sigma_x = \sigma_y = 0.5$ and $\sigma_{px} = \sigma_{py} = 1.0$ on the excited surface of the potential of eq 35 (which is shown in Figure 6). The initial momentum is $(p_x,p_y) = (10,0)$. (c and d) Same distribution only now for dynamics as calculated with A-FSSH using a swarm of 20 000 trajectories sampled from the initial Wigner distribution. Populations of fragments A−E are given in Table 1.

to outperform FSSH. Because reflecting trajectories proceed through two avoided crossings—where we would expect to see spurious effects from overly or underly coherent amplitudes—this data suggests that the A-FSSH algorithm applies an appropriate amount of decoherence.

Finally, Figure 5 demonstrates, surprisingly, that phase-corrected A-FSSH is able to describe a large number of resonances accurately. These resonances are quantum effects, and it is remarkable that a classical model can achieve such accuracy. At the same time, however, note that without decoherence, phase-corrected A-FSSH yields very poor branching ratios for reflection on the upper surface, worse than even standard FSSH. This implies that when applying Shenvi's phase correction, decoherence is especially important following the well-known rule in quantum mechanics that phase and decoherence are intimately related.

Altogether, from these two model problems (X and S) we conclude that (i) the A-FSSH scheme for decoherence can now treat the case of more than two electronic states quite well and (ii) when implemented with the phase correction of Shenvi[2] (eq 15) we can nearly match exact results in one dimension, even when there are some recoherent events. In the next subsection, we will explore the generality of these results for systems with multiple nuclear dimensions.

III.B. Wave Packet Separation in Two Nuclear Dimensions. In order to investigate the effects of decoherence on a wave packet in multiple nuclear dimensions, we now investigate a new Hamiltonian with two electronic states and two nuclear degrees of freedom

$$\begin{aligned} V_{11} &= -F\tanh(Bx) \\ V_{22} &= A\tanh(z) + 3A/4 \\ z &= B(x-1) + W\cos(Gy + \pi/2) \\ V_{12} &= C\exp(-Dx^2) \end{aligned} \tag{35}$$

The parameters we choose are A = 0.2, B = 0.6, C = 0.015, $F = A/4$, D = 0.3, G = 0.3, and W = 2, all in atomic units. Contours of the potential energy surface are shown in Figure 6. At time t = 0, we imagine a Gaussian wave packet with width $\sigma_x = \sigma_y = 0.5$ and $\sigma_{px} = \sigma_{py} = 1.0$ at position (x_0,y_0) on the upper adiabatic surface. In Figure 6, we draw the wave packet in blue for the case $(x_0,y_0) = (-4,0)$. More generally, we calculated results for $x_0 = -4$ and $y_0 = -2, -1, 0, 1$, or 2. The initial momentum is $(p_x,p_y) = (10,0)$.

As time moves forward, we propagate the Gaussian wave packet and watch it approach the region of derivative coupling. In Figure 6, we show the sequence of events that follow. During the first encounter with the region of derivative coupling, the wave packet spawns two new Gaussian wave packets on the lower adiabatic surface, which we label "C" and "D". After this initial spawning event, the initial wave function on the upper surface continues to move along and interact with its evolving image on the lower adiabatic surface. Eventually, when the wave packet reaches another turning point, two more wave packets are spawned on the lower surface, labeled "A" and "B". Finally, the wave packet remaining on the upper surface reflects and moves backward (toward $x \rightarrow -\infty$), leading to fragment "E". We stop all time propagation at time t = 2300 au.[44]

In Figure 7, we make contour plots of the A, B, C, D, E fragments using both exact (grid-based) quantum dynamics and the A-FSSH algorithm. Similar plots can be made using any of the other surface-hopping schemes above. The key observation here is that the Gaussian nature of the emerging wave packets is preserved using the surface-hopping algorithm, and this model problem allows us to quantify not just branching ratios (or populations) on the different electronic surfaces but also the distribution of the nuclear wave packets in phase space. To that end, in Table 1, we list the populations of each of these diverging fragments using the different surface-hopping schemes described above.

At the bottom of Table 1, we compute two different notions of error. First, we compute the averaging branching errors as the root-mean-square error for the population on the ground state

$$\text{avg. branching error} = \sqrt{\frac{\sum_{r_0}(\Delta\rho^{\text{total}}(r_0))^2}{5}} \tag{36}$$

dx.doi.org/10.1021/jp206557h |J. Phys. Chem. A 2011, 115, 12083–12096

Table 1. Total and Fragment Populations Found for the Different Wave Packets Emerging on the Ground State in Figure 6[a]

starting position $r_0 = (x_0,y_0)$	fragment in ground state	exact population (ρ)	A-FSSH (Std.) error ($\Delta\rho$)	FSSH (Std.) error ($\Delta\rho$)	A-FSSH (phase-corr.) error ($\Delta\rho$)	FSSH (phase-corr.) error ($\Delta\rho$)	A-FSSH (std.) error ($\Delta\rho$)
	rescaling direction		$\vec{u}_{sc} = \vec{d}$	$\vec{u}_{sc} = \vec{d}$	$\vec{u}_{sc} = \vec{d}$	$\vec{u}_{sc} = \vec{d}$	$\vec{u}_{sc} = \delta\vec{P}$
(−4, −2)	total	0.9146	0.0009	0.0068	0.0168	0.0275	−0.0031
	A + B + C + D	0.9137	−0.0011	0.0061	0.0150	0.0268	−0.0058
	A	0.1179	0.0181	−0.0001	0.0275	0.0253	0.0080
	B	0.0493	0.0002	0.0155	−0.0091	0.0009	0.0008
	C	0.0287	−0.0050	0.0041	−0.0087	−0.0103	−0.0041
	D	0.7179	−0.0145	−0.0135	0.0052	0.0108	−0.0106
(−4, −1)	total	0.7425	0.0261	0.0690	0.0449	0.0604	0.0146
	A + B + C + D	0.7413	0.0257	0.0689	0.0045	0.0601	0.0042
	A	0.1052	0.0383	0.0367	0.0389	0.0380	0.0241
	B	0.1426	0.0039	0.0175	−0.0064	0.0079	0.0015
	C	0.0933	−0.0134	0.0123	−0.0164	−0.0165	−0.0142
	D	0.4033	−0.0063	−0.0009	0.0257	0.0275	−0.0104
(−4, 0)	total	0.5581	0.0581	0.1336	0.0691	0.1306	0.0455
	A + B + C + D	0.5524	0.0563	0.1322	0.0677	0.1285	0.0397
	A	0.0768	0.0572	0.0894	0.0584	0.0824	0.0446
	B	0.1707	0.0186	0.0138	0.0138	0.0110	0.0127
	C	0.1140	−0.0215	0.0257	−0.0172	0.0137	−0.0181
	D	0.1909	−0.0019	0.0032	0.0126	0.0212	0.0004
(−4, 1)	total	0.4525	0.0882	0.1608	0.1077	0.2018	0.0693
	A + B + C + D	0.4513	0.0872	0.1596	0.1046	0.1994	0.0688
	A	0.1139	0.0421	0.0791	0.0454	0.0890	0.0745
	B	0.0951	0.0462	0.0461	0.0509	0.0656	−0.0101
	C	0.0911	0.0091	0.0487	0.0099	0.0463	0.0043
	D	0.1512	−0.0104	−0.0144	−0.0016	−0.0015	0.0000
(−4, 2)	total	0.5117	0.0752	0.1463	0.1013	0.1856	0.0589
	A + B + C + D	0.5086	0.0713	0.1422	0.0971	0.1808	0.0588
	A	0.1641	0.0041	0.0633	0.0127	0.0563	0.0101
	B	0.0458	0.0525	0.0691	0.0595	0.0800	0.0203
	C	0.0991	0.0196	0.0214	0.0285	0.0419	0.0393
	D	0.1995	−0.0049	−0.0115	−0.0036	0.0026	−0.0108
	avg. branch. error	n/a	0.0591	0.1183	0.0760	0.1390	0.0460
	avg. pos. error	n/a	0.0522	0.0793	0.0579	0.0856	0.0477

[a] The particle begins on the excited state at $t = 0$, and we stop all time propagation at $t = 2300$ au.[44] The average errors (at the bottom) are defined in eqs 36 and 37.

Here, the sum over r_0 reflects a sum over the 5 different initial conditions for (x_0,y_0) in Table 1. Second, we also compute the average error in position according to the fragment populations on A, B, C, D

$$\text{avg. positional error} = \sqrt{\frac{\sum_{r_0}\sum_{\text{fragment}} \left(\Delta\rho^{\text{fragment}}(r_0)\right)^2}{5}} \qquad (37)$$

From the data in Table 1 we see that allowing for decoherence in this model system reduces the error in total branching ratios by up to a factor of 2: (i) without decoherence one finds ground state populations with errors up to 33%; (ii) with decoherence one finds that all branching errors are under 15%. This is a strong reminder that decoherence is crucial for predicting long-time dynamics where a particle encounters multiple regions of derivative coupling.

Interestingly, even though adding decoherence reduces the errors in total population (i.e., the average branching errors) by a factor of 2, adding decoherence reduces the errors in fragment populations (i.e., the average position errors) by only a factor 1.5. In other words, even though standard FSSH (without decoherence) does not predict the correct population on the ground state at the final time, it does predict decent fragment populations given this limitation. It is unclear how general this statement is; many more numerical studies examining this effect should certainly be explored in the future.

Finally, it is worth noting that unlike the cases in models S and X above, the phase correction does not yield significantly improved results for this Hamiltonian. In fact, for some cases the phase correction sometimes yields answers that are slightly worse than those obtained with the standard TDSE, even when decoherence is included. The implications of this result will be discussed in the next section.

IV. DISCUSSION

In this article, we focused on three key problems relating to surface hopping and decoherence. First, we extended the A-FSSH

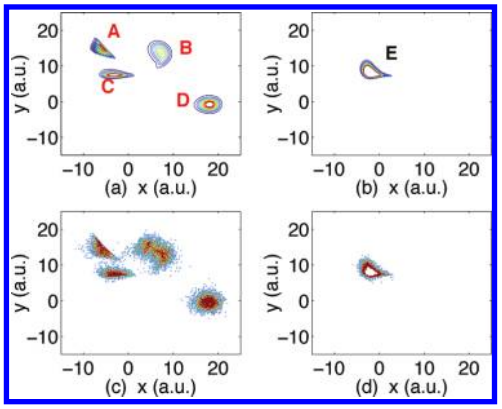

Figure 8. (a and b) Same as Figure 6a and 6b. (c and d) Positional distribution for a swarm of classical particles using the A-FSSH algorithm but rescaling momentum in the direction $\vec{u}_{sc} = \delta\vec{P}_{jj}$, where j is the surface accepting a hop. All parameters chosen as in Figure 7. On one hand, note that fragment B in this plot is more visually scattered and broadened compared with our results in Figure 7, suggesting that the direction of derivative coupling (i.e., $\vec{u}_{sc} = \vec{d}$) as suggested by Tully[3] is the better choice for rescaling direction. On the other hand, however, note that $\vec{u}_{sc} = \delta\vec{P}_{jj}$ yields slightly better branching ratios (see last column of Table 1).

scheme to more than two electronic states and showed that the resulting algorithm still captures the crucial physics of decoherence for long time dynamics. Second, we examined the effects of decoherence on a well-defined model Hamiltonian with two nuclear dimensions, where we can quantify not just populations but also the spatial distribution of the spawned wave packets. In this case, we find that decoherence improves both populations (strongly) and spatial distributions (moderately). Third, we rederived the phase-corrected equation of motion suggested by Shenvi and co-workers (in the Appendix) and applied eq 15 to the same model problems described above. For the phase-corrected algorithm, we find significant improvement in all one-dimensional problems but no improvement for the two-dimensional Hamiltonian.

Regarding the extension of A-FSSH into multiple electronic and nuclear degrees of freedom, the results of this work are encouraging: thus far, all evidence suggests that one can model higher dimensional coupled nuclear−electronic problems using A-FSSH, i.e., the decoherence rate still gives a meaningful and valid correction. In the past few months alone the FSSH algorithm has been used in several pioneering publications probing electronic relaxation after photoexcitation (e.g., refs 45−48), and in the future, it will be very interesting to investigate the effects of decoherence on these published model systems. Before concluding, we now want to address two important issues in the A-FSSH algorithm.

IV.A. Phase Correction in Many Dimensions. Regarding the phase correction of Shenvi and co-workers,[2] our results are mixed. On the one hand, Figures 2−5 demonstrate conclusively that for one-dimensional models the phase-corrected algorithm performs phenomenally, usually matching exact quantum results perfectly. On the other hand, for the two-dimensional model the phase correction does not yield a substantial improvement and sometimes performs a bit worse than the standard TDSE (see Table 1). This being said, the data from ref 2 demonstrates that for another two-dimensional model Hamiltonian the phase-corrected surface-hopping algorithm yields extremely good results (effectively exact), far better than the standard FSSH results. In summary, a lot more benchmarking is needed for understanding when and how the phase-corrected algorithm succeeds and the limitations of the corresponding parallel momentum approximation (eq 16).

To that end, in a set of preliminary calculations on the two-dimensional model problem in section III.B, we explored going beyond the parallel momentum assumption in eq 16 using the moments $\delta\vec{P}$ to generate the virtual momenta in eq 15. Having done so, we do find noticeable improvements in our final branching ratios. Before any conclusions can be drawn, however, a great deal more benchmarking is needed.

IV.B. Momentum Rescaling. According to the standard FSSH algorithm, when a hop occurs between adiabatic surfaces ($i \rightarrow j$), one must scale the momentum in some direction $\vec{u}_{sc}$, as in eq 30. Tully proposed[3] that the best option for $\vec{u}_{sc}$ is to choose the direction of the derivative coupling, $\vec{u}_{sc} = \vec{d}_{ij}$. In order to test the validity of this ansatz, we performed A-FSSH calculations where, as an alternative rescaling direction, we choose the direction of the first momentum moment: $\vec{u}_{sc} = \delta\vec{P}_{jj}$. Note that if i is the active surface, then $\delta\vec{P}_{ii} \approx 0$ so that this direction is virtually identical to $\vec{u}_{sc} = \delta\vec{P}_{jj} - \delta\vec{P}_{ii}$ (which we suggested in ref 1, only now in a slightly simpler form).

Unfortunately, our final results are ambiguous. On one hand, for this new choice of momentum rescaling direction we do find better branching ratios (see last column in Table 1). On the other hand, to the naked eye the spatial distributions of our results in Figure 8 are clearly inferior to the results found by rescaling in the direction of the derivative coupling. Comparing Figures 8 and 7 and focusing on fragment B, one sees that this new rescaling direction leads to much more scattered and delocalized position distributions (which do not resemble the exact results). We attribute this to the fact that the momentum moment reflects the history of the particle rather than just the local information at the instantaneous position. In the end, considering all of our data we tentatively hypothesize that the direction of the derivative coupling is overall a better option for momentum rescaling, but this is not yet a firm conclusion.

V. CONCLUSIONS

This paper provides a route for adding decoherence to the surface-hopping algorithm in higher dimensionality (nuclear and electronic) and a new set of model problems for measuring progress along that journey. Thus far, the A-FSSH algorithm offers a stable and meaningful decoherence correction to the surface-hopping algorithm, and we hope this article will help encourage the computational chemistry community to experiment with decoherence in their own surface-hopping calculations, especially for problems with high dimensionality.

■ APPENDIX

A. Rescaling Moments after Hops and Collapsing Events. To complete our discussion of the A-FSSH algorithm, we now consider how to treat all moments (position and momentum) after discontinuous hopping and collapsing events.

1. Moments and Collapsing Events. First, we consider collapsing events. Suppose we are propagating our nuclear coordinates $(\vec{R},\vec{P})$ along surface i. In a basis of adiabatic electronic states, $\{|\Phi_l\rangle\}$, the electronic wave function is

represented by $\vec{c}\,(t)$

$$|\Psi^{\mathrm{el}}(t)\rangle = \sum_l c_l(t)|\Phi_l\rangle \tag{38}$$

and we have moments $\delta\vec{R}$,$\delta\vec{P}$. Within the A-FSSH algorithm, we consider a collapsing event to be an event that occurs when a fictitious wave packet moving along another surface, say $k \neq i$, moves away from the primary wave packet, so the two wave packets are no longer interacting. In such a case, we need to collapse the electronic wave function to eliminate the electronic amplitude on adiabatic state k. The result is eq 32.

How can we treat the moments after a collapsing event? Certainly, the moments associated with state k should be set to zero

$$\delta\vec{R}_{jk}^{\,\mathrm{new}} = \delta\vec{R}_{kj}^{\,\mathrm{new}} = 0\;\forall\, j \tag{39}$$

$$\delta\,\vec{P}_{jk}^{\,\mathrm{new}} = \delta\,\vec{P}_{kj}^{\,\mathrm{new}} = 0\;\forall\, j \tag{40}$$

We next choose to recenter all wave packet moments so that the particle on the active surface i has a zero moment. To that end, we propose to displace all moments in the direction of $(\delta\vec{R}_{ii},\delta\vec{P}_{ii})$

$$\delta\vec{R}_{jj}^{\,\mathrm{new}} = \delta\vec{R}_{jj} - \lambda_j\delta\vec{R}_{ii} \quad j \neq k \tag{41}$$

$$\delta\,\vec{P}_{jj}^{\,\mathrm{new}} = \delta\,\vec{P}_{jj} - \lambda_j\delta\,\vec{P}_{ii} \quad j \neq k \tag{42}$$

Ideally, we would like to set $\lambda_j = \sigma_{jj}/\sigma_{ii}$ to preserve the distances between virtual wave packet centers. Unfortunately, this expression is not necessarily stable for small σ_{ii}, so we are forced to make an approximation for numerical stability:

$$\lambda_j = \min\left(1, \frac{\sigma_{jj}}{\sigma_{ii}}\right) \tag{43}$$

It is essential that, by the above procedure, unpopulated states are not disturbed by unrelated collapsing events. In other words, if before a collapsing event an electronic state (say n) has $\sigma_{nn} = \delta R_{nn} = \delta P_{nn} = 0$, then afterward we still have $\sigma_{nn} = \delta R_{nn} = \delta P_{nn} = 0$, a crucial property for doing multistate dynamics. This gives us a complete prescription for treating multiple electronic states during a collapsing event.

2. Moments and Hops. Second, we now turn to the question of hopping events. As before, we suppose the FSSH trajectory is propagating along surface i, but now we want to hop to surface j. According to standard FSSH dogma, during a hop, the electronic amplitudes are left unchanged, as is the coordinate $\vec{R}$. The momentum $\vec{P}$ is scaled in some normalized direction $\vec{u}_{sc}$ (e.g., the direction of derivative coupling) in order to conserve energy, as in eq 30.

What should be done with the moments after a hop? For a consistent treatment of moments and trajectories, we would like to leave the position moments unchanged (thus preserving the distances between virtual wave packet centers) while rescaling only momentum moments. At the same time, we would also like to recenter all moments correctly relative to surface j. These two goals are not fully compatible in practice. In particular, the only way to preserve the distances between wave packet centers is to shift all position moments by a displacement $\delta R_{jj}/\sigma_{jj}$. However, just as we saw in eqs 41 and 42, this displacement vector can be unstable as a hop can occur when an electronic state has gained only infinitesimal population, so that σ_{jj} is nearly zero. With this in mind, for purposes of rescaling, we will scale the position moments as follows

$$\delta\vec{R}_{nn}^{\,\mathrm{new}} = \delta\vec{R}_{nn} - \lambda_n\sigma_{nn}\delta\vec{R}_{jj} \tag{44}$$

and we will insist that $\lambda \geq 1$ (since $1/\sigma_{jj} > 1$). Now, to specify our exact choice of λ, we choose to minimize the final moment relative to the active surface, which should minimize the final decoherence rate. The appropriate choice of λ with this criterion is

$$\lambda_n = \max\left\{1, \frac{\delta\vec{R}_{nn}\cdot\delta\vec{R}_{jj}}{\sigma_{nn}(\delta\vec{R}_{jj}\cdot\delta\vec{R}_{jj})}\right\} \tag{45}$$

Equation 45 ensures that after a hop to surface j, $\delta R_{jj}^{\alpha} = 0\;\forall\alpha$.

Although eq 45 is not a perfect means to scaling position moments, the end result will be a smaller than optimal decoherence rate. In other words, after a hop occurs, we are making the moments less in absolute value than they should be and since the decoherence rate is roughly proportional to the moment sizes, our calculated decoherence rate should be smaller than optimal. However, since standard FSSH has no decoherence rate at all, our A-FSSH result should certainly improve upon bare FSSH results. Most importantly, by using eqs 44 and 45, we gain complete computational stability, which is more than worth any potential cost.

Our last order of business is how to rescale the momentum moments after a hop. Just as the momentum itself is rescaled in some direction $\vec{u}_{sc}$ by conservation of energy, we seek a similar treatment for the momentum moments. With that goal in mind, we introduce a factor η_n to be multiplied by the direction of momentum adjustment, $\vec{u}_{sc}$:

$$\delta P_{nn}^{\alpha,\,\mathrm{new}} = \delta P_{nn}^{\alpha} - \eta_n u_{sc}^{\alpha} \tag{46}$$

To determine η_n, we now force the amplitude on each potential energy surface to obey conservation of energy

$$\sum_\alpha \frac{\left[P^\alpha + \left(\frac{\delta P_{nn}^\alpha - \eta_n u_{sc}^\alpha}{\sigma_{nn}}\right)\right]^2}{2M^\alpha} + V_{nn}\left(\vec{R} + \frac{\delta\vec{R}_{nn}^{\,\mathrm{new}}}{\sigma_{nn}}\right) = E_{\mathrm{tot}} \tag{47}$$

Lastly, in order to keep all equations local, we enforce eq 47 only to first order so that we find a quadratic equation for η_n

$$\eta_n^2 \sum_\alpha \frac{(u_{sc}^\alpha)^2}{2M_\alpha} - \eta_n \sum_\alpha \frac{(P^\alpha\sigma_{nn} + \delta P_{nn}^\alpha)u_{sc}^\alpha}{M^\alpha} + \left(\sum_\alpha \frac{(P^\alpha\sigma_{nn} + \delta P_{nn}^\alpha)^2}{2M^\alpha} + V_{nn}(\vec{R})\sigma_{nn}^2 - \sum_\alpha F_{nn}^\alpha \delta R_{nn}^{\alpha,\,\mathrm{new}}\sigma_{nn} - E_{\mathrm{tot}}\sigma_{nn}^2\right) = 0 \tag{48}$$

Equation 48 yields two roots for η_n, and we choose the root with smallest $|\eta_n|$. Equations 46 and 48 give a complete prescription for determining $\delta\vec{P}$ after a hop between surfaces. Note that, after a hop to surface j, in addition to $\delta R_{jj}^{\alpha} = 0$ we also have $\delta P_{jj}^{\alpha} = 0$.

B. Phase Correction from the Quantum Liouville Equation. Our final theoretical concern is the phase-corrected equation of motion for electronic amplitude. Originally,[2] Shenvi derived eq 15 from Heller's equations for propagating frozen Gaussians.[49] We now rederive this new equation of motion starting from the Liouville equation, so that the resulting equation will certainly be compatible with the A-FSSH algorithm. As always, we will propagate Tully's FSSH algorithm in an adiabatic basis.

We showed above in eq 11 that the standard TDSE is correct only to first order in $\delta\hat{R}$, $\delta\hat{P}$ for the total reduced density matrix. As an alternative variable of choice, consider a slightly different reduced density matrix

$$\begin{aligned}\hat{\sigma}(t) &= \mathrm{Tr}_N(\delta(\vec{\mathbf{R}} - \vec{R}_{SH}(t))\hat{\boldsymbol{\rho}}(t)) \\ &= \langle \vec{R}_{SH}(t)|\hat{\boldsymbol{\rho}}(t)|\vec{R}_{SH}(t)\rangle \end{aligned} \tag{49}$$

$$\sigma_{jk}(t) \equiv \langle \Phi_j \vec{R}_{SH}|\hat{\boldsymbol{\rho}}(t)|\Phi_k \vec{R}_{SH}\rangle \tag{50}$$

The difference between eq 1 and eq 49 is that the former considers the fully reduced electronic density matrix (i.e., the full trace over nuclei), while the latter considers the electronic density matrix evaluated at one specific point in phase space, $(\vec{R}_{SH}, \vec{P}_{SH})$. In order to find an equation of motion for this new reduced density matrix, we will assume that we are operating in a region of zero derivative coupling; later, we will generalize to regions with derivative coupling (in eq 68). With this assumption, if we take the derivative of eq 49 we find

$$\begin{aligned}\frac{\mathrm{d}}{\mathrm{d}t}\sigma_{jk}(t) &= \left\langle \Phi_j \vec{R}_{SH}(t)\middle|\frac{\mathrm{d}}{\mathrm{d}t}\hat{\boldsymbol{\rho}}(t)\middle|\Phi_k \vec{R}_{SH}(t)\right\rangle \\ &\quad + \left\langle \Phi_j \frac{\mathrm{d}}{\mathrm{d}t}\vec{R}_{SH}(t)|\hat{\boldsymbol{\rho}}(t)|\Phi_k \vec{R}_{SH}(t)\right\rangle \\ &\quad + \left\langle \Phi_j \vec{R}_{SH}(t)|\hat{\boldsymbol{\rho}}(t)|\Phi_k \frac{\mathrm{d}}{\mathrm{d}t}\vec{R}_{SH}(t)\right\rangle \end{aligned} \tag{51}$$

$$\begin{aligned} &= -\frac{i}{\hbar}\langle \Phi_j \vec{R}_{SH}(t)|[\hat{\mathbf{H}}, \hat{\boldsymbol{\rho}}]|\Phi_k \vec{R}_{SH}(t)\rangle \\ &\quad - \sum_\alpha \frac{P^\alpha_{SH}}{M^\alpha}\left\langle \Phi_j \frac{\partial}{\partial R^\alpha}\vec{R}_{SH}(t)|\hat{\boldsymbol{\rho}}(t)|\Phi_k \vec{R}_{SH}(t)\right\rangle \\ &\quad - \sum_\alpha \frac{P^\alpha_{SH}}{M^\alpha}\left\langle \Phi_j \vec{R}_{SH}(t)|\hat{\boldsymbol{\rho}}(t)|\Phi_k \frac{\partial}{\partial R^\alpha}\vec{R}_{SH}(t)\right\rangle \end{aligned} \tag{52}$$

$$\begin{aligned} &= -\frac{i}{\hbar}\langle \Phi_j \vec{R}_{SH}(t)|[\hat{\mathbf{H}}, \hat{\boldsymbol{\rho}}]|\Phi_k \vec{R}_{SH}(t)\rangle \\ &\quad + \frac{i}{\hbar}\sum_\alpha \frac{P^\alpha_{SH}}{M^\alpha}\langle \Phi_j \vec{R}_{SH}(t)|[\mathbf{P}^\alpha, \hat{\boldsymbol{\rho}}]|\Phi_k \vec{R}_{SH}(t)\rangle \end{aligned} \tag{53}$$

To arrive at eqs 52 and 53 we use the following manipulations, where we consider an infinitely narrow Gaussian χ to represent a delta function

$$\begin{aligned}&\left\langle \frac{\mathrm{d}\chi(\vec{R}_{SH}(t))}{\mathrm{d}t}\middle|\psi\right\rangle \\ &= \int \mathrm{d}\vec{R}\,\frac{\mathrm{d}\chi(\vec{R} - \vec{R}_{SH}(t))}{\mathrm{d}t}\psi(\vec{R}) \end{aligned} \tag{54}$$

$$= \sum_\alpha \frac{\mathrm{d}R^\alpha_{SH}}{\mathrm{d}t}\int \mathrm{d}\vec{R}\,\frac{\partial\chi(\vec{R} - \vec{R}_{SH}(t))}{\partial R^\alpha_{SH}}\psi(\vec{R}) \tag{55}$$

$$= -\sum_\alpha \frac{P^\alpha_{SH}}{M^\alpha}\int d\vec{R}\,\frac{\partial\chi(\vec{R} - \vec{R}_{SH}(t))}{\partial R^\alpha}\psi(\vec{R}) \tag{56}$$

$$= \sum_\alpha \frac{P^\alpha_{SH}}{M^\alpha}\int \mathrm{d}\vec{R}\chi(\vec{R} - \vec{R}_{SH}(t))\frac{\partial\psi(\vec{R})}{\partial R^\alpha} \tag{57}$$

$$= \sum_\alpha \frac{P^\alpha_{SH}}{M^\alpha}\left\langle \chi(\vec{R}_{SH}(t))\middle|\frac{\partial\psi}{\partial R^\alpha}\right\rangle \tag{58}$$

To simplify eq 53, we then use the decomposition $\hat{\mathbf{H}} = \hat{\mathbf{V}} + \mathbf{T}$, and recalling that V is diagonal because of our choice of an adiabatic basis, the result is

$$\begin{aligned}\frac{\mathrm{d}}{\mathrm{d}t}\sigma_{jk}(t) &= -\frac{i}{\hbar}(V_{jj} - V_{kk})\sigma_{jk} - \frac{i}{\hbar}\left\langle \Phi_j \vec{R}_{SH}(t)|[\mathbf{T}, \hat{\boldsymbol{\rho}}]|\Phi_k \vec{R}_{SH}(t)\right\rangle \\ &\quad + \frac{i}{\hbar}\sum_\alpha \frac{P^\alpha_{SH}}{M^\alpha}\left\langle \Phi_j \vec{R}_{SH}(t)|[\mathbf{P}^\alpha, \hat{\boldsymbol{\rho}}]|\Phi_k \vec{R}_{SH}(t)\right\rangle \end{aligned} \tag{59}$$

To proceed further, we make three additional assumptions. First, we assume that the full wave packet is a sum of frozen Gaussian nuclear wave packets, one on each adiabatic surface (eq 18). For adiabatic surface n, these Gaussians have positions $(\vec{R}_n, \vec{P}_n)$ in phase space. Accordingly, the density matrices become

$$\hat{\boldsymbol{\rho}}(t) = \int \mathrm{d}R \int \mathrm{d}R' \sum_{lm} c_l(t)c^*_m(t)g_l(R)g^*_m(R')|\Phi_l R\rangle\langle\Phi_m R'| \tag{60}$$

$$\Rightarrow \sigma_{jk}(t) = c_j(t)c^*_k(t)g_j(R_{SH})g^*_k(R_{SH}) \tag{61}$$

where $g_i(R)$ is defined in eq 19. It follows that

$$\begin{aligned}&\langle \Phi_j \vec{R}_{SH}(t)|[\mathbf{T}, \hat{\boldsymbol{\rho}}]|\Phi_k \vec{R}_{SH}(t)\rangle \\ &= c_j c^*_k \sum_\alpha \frac{-\hbar^2}{2M^\alpha}\left(\frac{\partial^2 g_j}{\partial(R^\alpha)^2}g^*_k - g_j\frac{\partial^2 g^*_k}{\partial(R^\alpha)^2}\right)\Bigg|_{\vec{R}=\vec{R}_{SH}} \end{aligned} \tag{62}$$

Second, we assume that the zero-point energy is much less than the kinetic energy, effectively making a quasi-classical ansatz. Third, we assume that all frozen Gaussians are centered at position $\vec{R}_{i,j} = \vec{R}_{SH}\ \forall i, j$, even though they must have different momenta for enery conservation $(\vec{P}_i \neq \vec{P}_j)$. With these assumptions, we find

$$\langle \Phi_j \vec{R}_{SH}(t)|[\mathbf{T}, \hat{\boldsymbol{\rho}}]|\Phi_k \vec{R}_{SH}(t)\rangle = \sigma_{jk}\sum_\alpha \frac{(P^\alpha_j)^2 - (P^\alpha_k)^2}{2M^\alpha} \tag{63}$$

so that

$$-\frac{i}{\hbar}(V_{jj}-V_{kk})\sigma_{jk}-\frac{i}{\hbar}\langle\Phi_j\vec{R}_{SH}(t)|[\mathbf{T},\hat{\boldsymbol{\rho}}]|\Phi_k\vec{R}_{SH}(t)\rangle = 0 \tag{64}$$

by conservation of energy (see eq 17).

Thus, we may conclude that

$$\frac{\mathrm{d}}{\mathrm{d}t}\sigma_{jk}(t) = \frac{i}{\hbar}\sum_\alpha \frac{P^\alpha_{SH}}{M^\alpha}\langle\Phi_j\vec{R}_{SH}(t)|[\mathbf{P}^\alpha,\hat{\boldsymbol{\rho}}]|\Phi_k\vec{R}_{SH}(t)\rangle \tag{65}$$

$$= c_j c_k^* \sum_\alpha \frac{P^\alpha_{SH}}{M^\alpha}\left(\frac{\partial g_j}{\partial R^\alpha}g_k^* + g_j\frac{\partial g_k^*}{\partial R^\alpha}\right)\Bigg|_{\vec{R}=\vec{R}_{SH}} \tag{66}$$

$$= \frac{i}{\hbar}\sigma_{jk}\sum_\alpha \frac{P^\alpha_{SH}}{M^\alpha}(P^\alpha_j - P^\alpha_k) \tag{67}$$

Lastly, if we now relax our constraint that the derivative coupling is strictly zero and we take into account the fact that the adiabatic electronic states can depend on nuclear position, the simplest correction is to take the time derivative of Φ_j and Φ_k in eq 50. As a result, we find

$$\frac{\mathrm{d}}{\mathrm{d}t}\sigma_{jk}(t) = \frac{i}{\hbar}\sigma_{jk}\sum_\alpha \frac{P^\alpha_{SH}}{M^\alpha}(P^\alpha_j - P^\alpha_k) - \sum_\alpha \frac{P^\alpha_{SH}}{M^\alpha}[\hat{d}^\alpha,\hat{\sigma}]_{jk} + \ldots \tag{68}$$

Equation 68 represents a new equation of motion for the electronic density matrix (rather than the usual TDSE). As might be expected, however, this equation leads to a mixed density matrix. In order to find a pure density matrix that approximates $\hat{\sigma}$, we make an approximation and propagate only those off-diagonal elements where one index corresponds to the active surface. In other words, if the active surface is i, we propagate only σ_{ij} and σ_{ji} as well as all diagonal elements σ_{jj}. The resulting matrix elements correspond to an electronic amplitude whose equation of motion is precisely eq 15, i.e., Shenvi's phase correction.

AUTHOR INFORMATION

Corresponding Author

*E-mail: subotnik@sas.upenn.edu.

ACKNOWLEDGMENT

I thank Neil Shenvi for fascinating and crucial conversations, as usual. J.E.S. was supported by the Air Force Young Investigator Program, AFOSR grant FA9550-11-0092.

REFERENCES

(1) Subotnik, J. E.; Shenvi, N. *J. Chem. Phys.* **2011**, *134*, 24105.
(2) Shenvi, N.; Subotnik, J. E.; Yang, W. *J. Chem. Phys.* **2011**, *135*, 24101.
(3) Tully, J. C. *J. Chem. Phys.* **1990**, *93*, 1061–1071.
(4) Tully, J. C. *Faraday Discuss.* **1998**, *110*, 407–419.
(5) Schmidt, J. R.; Parandekar, P. V.; Tully, J. C. *J. Chem. Phys.* **2008**, *129*, 44104.
(6) Martinez, T. J.; Ben-Nun, M.; Levine, R. D. *J. Phys. Chem.* **1996**, *100*, 7884–7895.
(7) Ben-Nun, M.; Martinez, T. J. *J. Chem. Phys.* **2000**, *112*, 6113–6121.
(8) Fang, J. Y.; Hammes-Schiffer, S. *J. Phys. Chem. A* **1999**, *103*, 9399–9407.
(9) Subotnik, J. E.; Shenvi, N. *J. Chem. Phys.* **2011**, *134*, 244114.
(10) Webster, F.; Rossky, P. J.; Friesner, R. A. *Comput. Phys. Commun.* **1991**, *63*, 494–522.
(11) Webster, F.; Wang, E. T.; Rossky, P. J.; Friesner, R. A. *J. Chem. Phys.* **1994**, *100*, 4835–4847.
(12) Schwartz, B. J.; Bittner, E. R.; Prezhdo, O. V.; Rossky, P. J. *J. Chem. Phys.* **1996**, *104*, 5942.
(13) Wong, K. F.; Rossky, P. J. *J. Chem. Phys.* **2002**, *116*, 8418–8428.
(14) Wong, K. F.; Rossky, P. J. *J. Chem. Phys.* **2002**, *116*, 8429–8438.
(15) Prezhdo, O. V.; Rossky, P. J. *J. Chem. Phys.* **1997**, *107*, 825–834.
(16) Prezhdo, O. V. *J. Chem. Phys.* **1999**, *111*, 8366.
(17) Fang, J. Y.; Hammes-Schiffer, S. *J. Chem. Phys.* **1999**, *110*, 11166–11175.
(18) Volobuev, Y. L.; Hack, M. D.; Topaler, M. S.; Truhlar, D. G. *J. Chem. Phys.* **2000**, *112*, 9716–9726.
(19) Hack, M. D.; Truhlar, D. G. *J. Chem. Phys.* **2001**, *114*, 2894–3002.
(20) Jasper, A. W.; Hack, M. D.; Truhlar, D. G. *J. Chem. Phys.* **2001**, *115*, 1804–1816.
(21) Zhu, C.; Jasper, A. W.; Truhlar, D. G. *J. Chem. Phys.* **2004**, *120*, 5543–5547.
(22) Zhu, C.; Nangia, S.; Jasper, A. W.; Truhlar, D. G. *J. Chem. Phys.* **2004**, *121*, 7658–7670.
(23) Jasper, A. W.; Truhlar, D. G. *J. Chem. Phys.* **2005**, *123*, 064103.
(24) Bedard-Hearn, M. J.; Larsen, R. E.; Schwartz, B. J. *J. Chem. Phys.* **2005**, *123*, 234106.
(25) Larsen, R. E.; Bedard-Hearn, M. J.; Schwartz, B. J. *J. Phys. Chem. B* **2006**, *110*, 20055–20066.
(26) Subotnik, J. E. *J. Chem. Phys.* **2010**, *132*, 134112.
(27) Kapral, R.; Ciccotti, G. *J. Chem. Phys.* **1999**, *110*, 8919–8929.
(28) Nielsen, S.; Kapral, R.; Ciccotti, G. *J. Chem. Phys.* **2000**, *112*, 6543–6553.
(29) Grunwald, R.; Kelly, A.; Kapral, R. In *Energy Transfer Dynamics in Biomaterial Systems*; Burghardt, I., Ed.; Springer-Verlag: Berlin, 2009; p 383.
(30) Aleksandrov, I. V. *Z. Naturforsch* **1981**, *36a*, 902.
(31) Boucher, W.; Traschen, J. *Phys. Rev. D* **1988**, *37*, 3522–3532.
(32) Zhang, W. Y.; Balescu, R. *J. Plasma Phys.* **1988**, *40*, 199–213.
(33) Balescu, R.; Zhang, W. Y. *J. Plasma Phys.* **1988**, *40*, 215–234.
(34) Anderson, A. *Phys. Rev. Lett.* **1995**, *74*, 621–625.
(35) Prezhdo, O. V.; Kisil, V. V. *Phys. Rev. A* **1997**, *56*, 162–175.
(36) Martens, C. C.; Fang, J. Y. *J. Chem. Phys.* **1997**, *106*, 4918–4930.
(37) Donoso, A.; Martens, C. C. *J. Phys. Chem. A* **1998**, *102*, 4291–4300.
(38) Micha, D. A.; Thorndyke, B. *Int. J. Quantum Chem.* **2002**, *90*, 759.
(39) Shenvi, N.; Subotnik, J. E.; Yang, W. *J. Chem. Phys.* **2011**, *134*, 144102.
(40) Horsfield, A. P.; Bowler, D. R.; Fisher, A. J.; Todorov, T. N.; Sanchez, C. G. *J. Phys.: Condens. Matter* **2004**, *16*, 8251.
(41) Horsfield, A. P.; Bowler, D. R.; Fisher, A. J.; Todorov, T. N.; Sanchez, C. G. *J. Phys.: Condens. Matter* **2005**, *17*, 4793.
(42) Stella, L.; Meister, M.; Fisher, A. J.; Horsfield, A. P. *J. Phys.: Condens. Matter* **2007**, *127*, 214104.
(43) Yang, S. D.; Coe, J. D.; Kaduk, B.; Martinez, T. J. *J. Chem. Phys.* **2009**, *130*, 134113.
(44) For the case $(x_0,y_0) = (-4,2)$, we ran the calculations until time $t = 2650$ au to increase the separation between fragments.
(45) Nelson, T.; Fernandez-Alberti, S.; Chernyak, V.; Roitberg, A. E.; Tretiak, S. *J. Phys. Chem. B* **2011**, *115*, 5402–5414.
(46) Nachtigallova, D.; Aquino, A. J. A.; Szymczak, J. J.; Barbatti, M.; Hobza, P.; Lischka, H. *J. Phys. Chem. A* **2011**, *115*, 5247–5255.
(47) Sheps, L.; Miller, E. M.; Horvath, S.; Thompson, M. A.; Parson, R.; McCoy, A. B.; Lineberger, W. C. *Science* **2010**, *328*, 220–224.
(48) Sheps, L.; Miller, E. M.; Horvath, S.; Thompson, M. A.; Parson, R.; McCoy, A. B.; Lineberger, W. C. *J. Chem. Phys.* **2011**, *134*, 184311.
(49) Heller, E. J. *J. Chem. Phys.* **1975**, *62*, 1544–155.